Compressible Fluid Model of Heavy Ion Collision

D. Mundinger and G. Bertsch

We have made a macroscopic description of heavy ion collisions based on the dynamics of an interacting Fermi fluid. This framework is general enough to permit the study of some of the bulk properties of the medium such as the stress tensor and the equation of state.

The degrees of freedom that we emphasize are the centers of the two nuclei, and the location of two boundaries which separate the nuclear matter into a compressed region and two uncompressed regions. These boundaries are assumed to be planar. Using the equation of state, along with the conservation laws for mass and momentum, we can generate equations of motion for each of the dynamical variables. The momentum transport between the two nuclei is taken from the theory of a collisionless interacting Fermi gas.[1] The flux of momentum along the radial direction is related to the density via the nuclear matter equation of state. The tangential component is independent of interactions and given by the window formula[2]

$$\frac{dP}{dAdt} = \int d^3p\, p_\perp v_\parallel f(p)$$

The Coulomb force is calculated from point charges and the surface tension is taken from the empirical surface energy. No shape degrees of freedom have been considered except in the formation of a neck region between the two separating nuclei This is taken to be a cylindrical tube with a radius given by the maximum overlap of the two nuclei.

Figure 1 shows several time slices in the evolution of a typical scattering event. The collision can be divided into three phases During phase one which starts at the moment of impact a region of higher density forms at the center and expands outward as the uncompressed matter flows inward. When the boundary of the compressed zone reaches the outer edge it is reflected back toward the center beginning phase two. The uncompressed matter has an outward velocity which gives rise to a rarefaction when the boundary reaches the middle. If the rarefaction is intense, the density may drop so low in the third phase that the fluid becomes unstable and the nuclear system breaks up. This behavior was studied previously in a one-dimensional model.[3] During the breakup phase there can be a significant momentum transfer because of the finite amount of time required for the instability to develop. We have used the results of our one-dimensional calculations to parameterize this breakup.

Qualitatively, the results are in accord with the more computer-intensive TDHF calculations In figure 2 we show the time evolution of the reaction $^{208}Pb + {}^{208}Pb$. The x's represent the

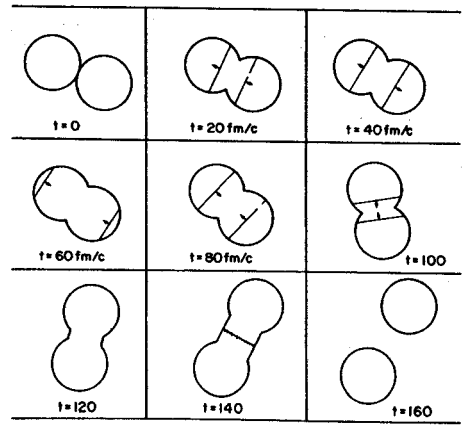

FIG. 1. Collision between two ^{118}Pd nuclei at an energy of 5 MeV/n (c.m.). The straight line represents the boundary between the two zones. The small arrows indicate its direction of motion.

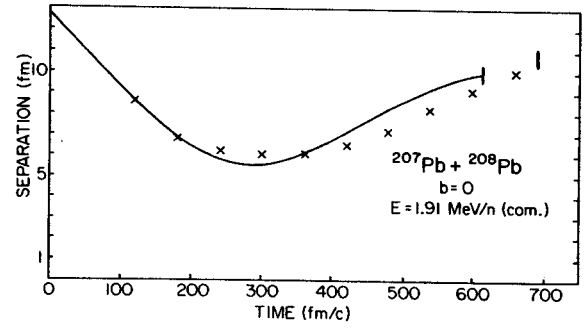

FIG 2. The distance between centers of two ^{208}Pb nuclei as a function of time. The line at the end indicates break up. Solid line: our calculation; dashed line: the TDHF calculation of ref. 4.

TDHF result.[4] The histories are practically identical except at the separation point. Here the TDHF solution has a sharply contracting neck while the fixed neck of our model slows the motion down more. The fusion region for a typical system is shown in figure 3. As in the TDHF results and in the model of Broglia, et al.,[5] we find a region of energy where fusion is limited to intermediate impact parameters. Fusion persists to higher energies in our model than in TDHF. Part of this is certainly due to our unrealistic fixed width neck. The energy loss for collisions in this low ℓ window are comparable in our model and TDHF.[6] In figure 4 we compare the final state energy in the reaction $^{40}Ca + {}^{40}Ca$ for a given low ℓ window size. At energies above the fusion

regime we find large energy dissipation at intermediate impact parameters, but rather little for head-on collisions. As in other approaches, we find deflection functions with negative angle rainbows in light systems. For heavier nuclei the rainbow moves to positive forward angles.

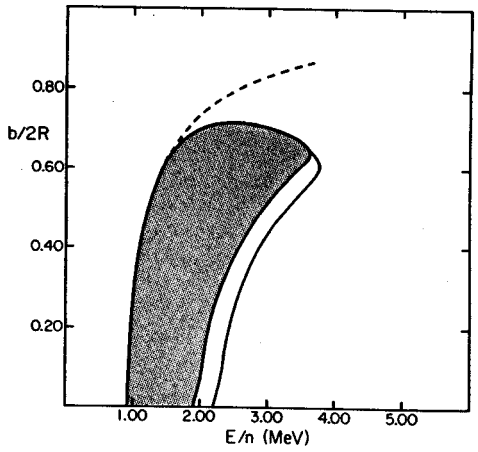

FIG. 3. The fusion region for the reaction $^{40}Ca(^{40}Cu, ^{80}Zr)$. The dashed line represents a grazing Coulomb trajectory. For an equation of state with K = 200 fusion takes place in the textured area. The area is enlarged as indicated for K = 500.

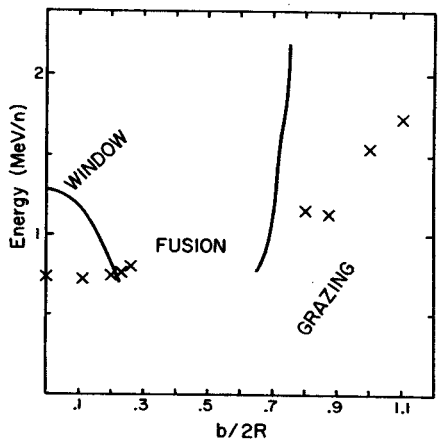

FIG. 4. Final state energies in the reaction $^{40}Ca(^{40}Ca + ^{40}Ca)^{40}Ca$. The Coulomb barrier in our model is at .85 MeV/n. The incident energy in the TDHF study is 1.738 MeV/n. To keep the same window we use an energy of 2.1 MeV/n.

We have varied the equation of state over the compressibility range of K = 200 - 500 MeV, and examined the effect on the observables. The fusion regime is increased in size with a stiffer equation of state. The effect is quite small however. There is also a negligible effect of the equation of state on the deflection functions. This accords with the finding of hydrodynamic calculations, that the transverse momentum transfer does not depend significantly on the equations of state.[7]

We can also include effects of nucleon-nucleon collisions in the momentum transport. If we assume that the pressure tensor relaxes to isotropy with a time constant given by[8]

$$\tau = \frac{1000 \text{ fm/c MeV}}{E_{lab} - V_{coul}},$$

we find a small increase in the energy dissipation and an increase in the fusion region of about 10% The next step in this program is to include the neck radius as an additional degree of freedom. This should improve the agreement with TDHF on the size of the fusion regime, and should move the rainbow to less forward angles. It will also permit the effect of two-body collisions on the transverse pressure to be realistically calculated.

---

1. G. Bertsch, in Nuclear Physics with Heavy Ions and Mesons, Les Houches, Session XXX, 1977. Edited by R. Balian, et al. (North Holland Publishing Company, 1978)
2. J.P. Blocki, et al., Ann. Phys. 113 (1978) 330.
3. G. Bertsch and D. Mundinger, Phys. Rev. C17 (1978) 1646.
4. A.K. Dhar and B S. Nilsson, Phys. Lett. 77B (1978) 50.
5 R.A. Broglia, et al., Phys. Lett. 53B (1974) 301.
6. H. Flocard and M.S. Weiss, Phys. Rev. C18 (1978) 573.
7. G. Bertsch and A. Amsden, Phys. Rev. C18 (1978) 1293.
8. G. Bertsch, Z. Physik A289 (1978) 103

Heavy Ion Reactions at Intermediate Energy

G. Bertsch, F. Serr, D. Mundinger

The theoretical description of heavy ion collisions at intermediate energy is still an open question. We have advocated[1] the theory based on Landau's kinetic equation,

$$\frac{\partial f}{\partial t} + v\cdot\nabla f \cdot \nabla U\cdot\nabla^{p} f = I.$$

The following equations result from taking moments of this equation in momentum space, and truncating at second order with a relaxation-time approximation.

$$\frac{D\rho}{Dt} + \rho(\nabla\cdot u) = 0 \quad \text{continuity}$$

$$\frac{Du}{Dt} + \nabla\cdot\overset{\approx}{S} + \nabla U\rho/m = 0 \quad \text{momentum}$$

$$\frac{DS^{ij}}{Dt} + \frac{(S^{ij} - 1/3S^{ij}\,\delta^{ij}\,\mathrm{tr}S/3)}{\tau} = -S^{ik}\,\nabla^{k}u^{j}$$

$$-S^{jk}\,\nabla^{k}u^{i} - S^{ij}(\nabla\cdot u) \quad \text{stress}$$

If the numerical solution of these two equations could be managed, it would be possible to infer from the experimental data the relaxation time τ and possibly the dependence of the mean field U on density.[2] Both these parameters are significant to discussions of phase transitions in nuclear matter.

Reported elsewhere in this volume are efforts to solve the equation by dividing the nuclei into zones of compression and of normal density. This method has the advantage that once the parameters describing the nuclei are chosen, the equations of motion are relatively simple. It has the disadvantage that the parameterization may be too constrained to yield reliable predictions.

The other method of attack which we are current pursuing is to make a general parameterization of the velocity field $\vec{u}$ and the stress components S^{ij} by a Fourier expansion. The differential equation for the components of S^{ij} can be solved directly in terms of $\vec{u}$. The equation of motion for $\vec{u}$ is solved by dotting the momentum equation into each of the Fourier component fields, and integrating over volume. This yields n simultaneous equations for the n Fourier components. The integration over nuclear volume will be done by dividing the total volume into elements, and keeping track of the position of each element by means of the velocity field $\vec{u}$.

---

1. G. Bertsch, Lecture notes for International School of Nuclear Physics, Erice, Italy, 1979.
2. G. Bertsch and A.A. Amsden, Phys. Rev. C18 1293 (1978).

Decay of Giant Vibrations

G. Bertsch

The decay of the giant vibrations is not well understood. Experimentally, there is a great deal of controversy about major decay modes.[1,2] On the theoretical side, the only decay branch that is relatively easy to calculate is nucleon emission. The RPA theory[3] predicts nucleon widths for the dipole and quadrupole vibrations that are considerably smaller than the experimental total width. The theory of alpha decay, the dominant decay mode in light nuclei, is in a much more primitive state. Shell model calculations have been made of the α-particle parentages of the excited state wave functions.[4] The alpha parentage is given in terms of harmonic oscillator wave functions, which must be joined onto continuum wave functions to calculate a width. We have done this part of the calculation using the Feshbach projection technique.[5] The computer program requires as input the oscillator wave function quantum numbers and size, the energy of the state, and the α-particle optical potential. Unfortunately, we find that the predicted widths are extremely sensitive to the assumed potential. Thus, at the present time we cannot make reliable calculations of alpha decay. We can get guidance, however, from the decay of $^{8}Be(2^{+})$, which surely provides an upper limit to α-widths. A fit to the phase shifts yields a width of 2 MeV. Thus, the experimental width of 6-8 MeV must be mainly due to damping into more complex configurations.

We have calculated damping in ^{208}Pb, making the 2p-2h doorway hypothesis for the final states.[6] Some qualitative conclusions that emerge are:

i) Typically, only a few states contribute to the damping, so the statistical limit is far from valid.

ii) RPA p-h correlations in the 2p-2h state are very important to achieve large damping widths.

iii) Predicted damping widths are somewhat low compared to experiment.

We are now investigating the predicted damping in other nuclei.

The study of decay angular distributions of the giant resonances reveals that most of the reaction can be regarded as knockout.[7] In previous work, we had concluded that knockout was relatively unimportant[8] on the basis of the RPA strength function with a discretized continuum. We need to reexamine this question, using the proper continuum representation of RPA, to determine conclusively the prediction of current theory.

---

1. M.T. Collins, et al., Phys. Rev. Letters 42, 1440 (1979).
2. J. van der Plicht, et al., Phys. Rev. Letters 42, 1121 (1979).
3. S. Shlomo and G. Bertsch, Nucl. Phys. A243, 507 (1975).
4. K.T. Hecht and D. Braunschweig, Nucl. Phys. A295, 34 (1978).
5. N. Auerbach, et al., Rev. Mod. Phys. 44, 48 (1972), eq. (A1.51).
6. G. Bertsch, et al., Phys. Lett. 80B, 163 (1979).
7. K.T. Knöfle, et al., Phys. Lett. 74B, 191 (1978).
8. S.F. Tsai and G.F. Bertsch, Phys. Rev. C11, 1634 (1975).

Pion Production in pp Collisions

D.O. Riska and J. Chai

The total cross section for $\pi^+ d \to pp$ and the angular distribution and asymmetry parameters for the inverse reaction $pp \to \pi^+ d$ with a polarized proton beam have been calculated with different models for the pion absorption and production operator and several sets of nuclear wavefunctions. The absorption operator includes both single nucleon and two-nucleon operators. Fair agreement can be achieved with all empirical parameters at low energies, but significant discrepancies occur at high energies. The results are very sensitive to the model for the nucleon-nucleon interaction used to generate the wavefunctions. The best results are achieved with the Reid soft core[1] and "Paris"[2] meson theory based nucleon-nucleon interactions.

1. J. Chai and D.O. Riska, "On the reactions $pp \to d\pi^+$, (in preparation).
2. R.V. Reid, Ann. Phys. 50, 411 (1978).
3. M. Lacombe et al., "Parameterization of the Paris N-N potential", Preprint IPNO/TH78-46, IPN Orsay 1978.

The Reactive Parts of the Pion-Nucleus Optical Potential

D.O. Riska, C.M. Ko, and J. Chai

The absorptive and dispersive parts of the second order pion-nucleus optical potential, proportional to ρ^2, have been calculated from a two-body model for the pion absorption mechanism. The S-wave part of the potential involves single pion rescattering and the P-wave part pion and rho meson rescattering. The absorptive parts at threshold, calculated with parameters that lead to good predictions of the total cross section for $\pi^+ d \to pp$, are somewhat smaller than the values favored in phenomenological analyses. The dispersive parts are less repulsive than the usual values. The energy dependence of the potential components is studied from threshold through the resonance region within the Fermi gas model.

1. C.M. Ko and D.O. Riska, "The absorptive P-wave pion-nucleus optical potential", Nucl. Phys. A312 217-235 (1978).
2. J. Chai and D.O. Riska, "The energy dependence of the absorptive S-wave pion-nucleus optical potential", Phys. Rev. C19, 1425 (1979).
3. J. Chai and D.O. Riska, "The reactive two-body part of the pion-nucleus optical potential", MSU preprint 1979.

The Role of the N^* (1688) Resonance on Nuclear Charge Form Factors

D.O. Riska

The pion exchange charge operator associated with excitation of an intermediate N^* (1688) resonance has been constructed. It was found that empirical information of resonant pion photoproduction amplitudes and quark model estimates for the γNN^* coupling strength indicate that this pion exchange charge operator is of far less significance for nuclear charge form factors than the pair exchange current.[1] The size of the effect depends strongly on the D-state admixtures in the wavefunctions. The result contradicts a recently published result by Kisslinger.[2]

1. D.O. Riska, "The effect of the N^* (1688) Resonance on Nuclear Charge Form Factors", MSU preprint 1979.
2. L.S. Kisslinger, "Experimental Tests of Isobar Components in Nuclei", in "Mesons in Nuclei", M. Rho and D. Wilkinson, eds., North Holland, Amsterdam, 1979, Vol. I, p. 261.

The Role of the Δ (1236) Pion Exchange Current on Total Photoabsorption Rates

D.O. Riska and H. Sarafian

Recent data on total photoabsorption rates in light nuclei show strong increases above the pion production threshold, and non-negligible cross sections also below that threshold. We have studied the contribution of the Δ (1236) exchange current to the total photoabsorption rate below the pion production threshold and found it to be appreciable.[1]

1. D.O. Riska, "Exchange Currents in Photo- and Electronuclear Reactions", in Proc. of the Conf. on Modern Trends in Elastic Electron Scattering, C. de Vries, ed., IKO, Amsterdam 1978, p. 119.

Model Independent Analysis of Scattering Experiments

Jerzy Borysowicz

The scattering experiments are usually analyzed by comparing the experimental cross section with the cross section predicted by a theoretical model. From this comparison one draws conclusions about the model. In the case of electron scattering on nuclei, it is possible to determine the charge density without using a physical model. Nevertheless certain general assumptions must be made. Borysowicz and Hetherington[1] have shown that quite weak and explicit assumptions about the density and form factor in the asymptotic regions allow determination of the density with the accuracy comparable with that achieved when stronger or more complicated assumptions are used.

Those methods are being applied to determine electric and magnetic densities of neutron, proton, ^{3}He, and ^{4}He.

We work now to extend the methods developed for the electron scattering to the case of proton scattering on nuclei. The important difference is that in the case of proton scattering there are always two unknown functions to be determined. The practical applications we consider are the determination of the optical potential for medium energy protons and determination of the profile function in Glauber approximation for high energy protons. Both the optical potential and the profile function have real and imaginary parts that have to be determined. Usually the problem is reduced to one unknown function by assuming that the real part of the optical potential is given or less directly in Glauber approximation that the proton density in a nucleus is known. We attempt here to proceed without making such an assumption. Although at the first sight it seems that the phase information is entirely lost and the problem is impossible to solve, the preliminary results indicate that it is possible to recover information about both functions.

---

1. J.R. Borysowicz and J.H. Hetherington, Nucl. Phys. A303, 425 (1978) and references therein.

E4 Transition Strengths

B.H. Wildenthal

The B(E4) values for excitations of the 0^+ ground states of the doubly even sd shell nuclei to the spectrum of 4^+ states in the first 10-15 MeV of excitation, together with some selected E4 excitations in the even-odd nuclei of this region, have been calculated from the Chung-Wildenthal $d_{1/2}$ - $s_{1/2}$ - $d_{3/2}$ wave functions. The aims are to predict the detailed distributions of E4 strength within each spectrum, to check the theoretical wave functions against experiment where data exist, and to extract an effective E4 charge if such a parametrization proves feasible. Preliminary results are shown in Table 1. It appears that the E4 strength is distributed in a more varied fashion than is the case for E2 strength. The relevant data are not extensive, but an isoscalar effective charge of $\tilde{e}_p + \tilde{e}_n = 2.0$ seems to be indicated.

Table 1. E4 transition strengths.

	$J_i \rightarrow J_f$	E_f (MeV) th	E_f (MeV) exp	$A\rho$[a]	$M\rho$[b]	B(E4)e^2fm 8 x 10^3 th	B(E4)e^2fm 8 x 10^3 exp
^{20}Ne	$0^+ \rightarrow 4^+(1)$	4.13	4.25	106.1	212	45	38 ± 8
	$4^+(2)$	9.86	9.03	- 20.2	- 40	1.6	
	$4^+(3)$	10.97		- 3.8	- 7.7	0.06	
	$4^+(4)$	11.70		- 1.1	- 2.3	0.0005	
^{24}Mg	$0^+ \rightarrow 4^+(1)$	4.42	4.12	- 19.7	39	1.6	2.0 ± 0.3
	$4^+(2)$	5.89	6.01	104.9	210	44	43 ± 6
	$4^+(3)$	8.79		12.5	25	0.6	
	$4^+(4)$	9.62		- 0.8	1.7	0.003	
^{28}Si	$0^+ \rightarrow 4^+(1)$	4.88	4.62	- 79.6	-159	25	18 ± 2
	$4^+(2)$	7.46	6.89	85.5	171	29	
	$4^+(3)$	9.67		16.4	33	1.1	
	$4^+(4)$	10.11		16.3	33	1.1	
^{32}S	$0^+ \rightarrow 4^+(1)$	4.82	4.46	-121.4	-243	59	
	$4^+(2)$	6.65	6.41	67.7	135	18	
	$4^+(3)$	7.55		20.0	40	1.6	
	$4^+(4)$	7.94		- 8.7	- 17	0.3	
^{36}Ar	$0^+ \rightarrow 4^+(1)$	4.74	4.41	-123.5	-248	62	
	$4^+(2)$	6.81		3.3	6.5	0.04	
	$4^+(3)$	9.07		- 30.5	- 61	37	
	$4^+(4)$	9.98		18.6	37	14	

[a] $A_n = A\rho$

[b] $M_n = M\rho$

M3 Transition Strengths

B.H. Wildenthal, B.A. Brown,
and W. Chung

Attention is currently focused upon a possible quenching of the M3 operator in the region of the sd shell, a quenching suggested by elastic electron scattering on ^{17}O and explained theoretically in terms of a correlation between the E2 isoscalar effective charge and the M3 isovector spin g-factor. The extant data on this topic are at present sparse, consisting of the results of a few moments extracted from elastic electron data and three transition rates measured for the only existing $\Delta J^{\pi} = 3^{+}$ transitions in the 16-40 region. However, future work with high-resolution electron accelerators should significantly augment this information, both in the measurements of ground state moments and of $0^{+} \rightarrow 3^{+}$ transitions in doubly-even nuclei.

Our initial analysis has been of the $3^{+} \rightarrow 0^{+}$ transitions in ^{34}Cl and the $1^{+} \rightarrow 4^{+}$ mirror transitions in ^{24}Al and ^{24}Na. In Table 1 the experimental values are compared to the predictions of the Chung-Wildenthal wave functions combined with the free nucleon estimates of the single-particle M3 matrix elements. It can be seen that while the relative values of the observed strengths are well reproduced, an overall quenching of the theoretical strengths appears to be needed. We are pursuing this issue in the context of a quenching of the single-particle matrix elements, in particular, a quenching of the isovector spin g-factor.

Table 1. B(M3) values (in units of $\mu_N^2 fm^4$) compared with the sd shell model predictions using free nucleon g factors.

Nucleus	^{24}Al	^{24}Na	^{34}Cl
$J_i \rightarrow J_f$	$1^{+} \rightarrow 4^{+}$	$1^{+} \rightarrow 4^{+}$	$3^{+} \rightarrow 0^{+}$
Exp	269 ± 13	1038 ± 5	16.8 ± 0.4
Th[a]	334	1538	26.0
Exp/Th	0.78	0.68	0.65

[a] Harmonic oscillator wave functions from ^{24}Mg and A = 34.

The extrapolation of the optical potential to higher energies is useful since there is much more data available near the resonance region. As described elsewhere (Ref. 1), we use phase shift values for b_0, b_1, c_0, c_1, and we use $\lambda = 1$. However, lacking any knowledge of the behaviour of the absorption parameters, we extrapolated them by comparison to phase shifts and the fitted values from pionic atoms.

The results from Chai and Riska (Ref. 2) allow the use of more theoretically reasonable numbers for the absorption parameters. A graph of these parameters is shown in Fig. 1, compared to the extrapolated values we had used before. Tables of the parameters may be found in Ref. 3. The absorption terms are also included in the Lorenz-Lorenz Ericson-Ericson effect, as described in the previous article.

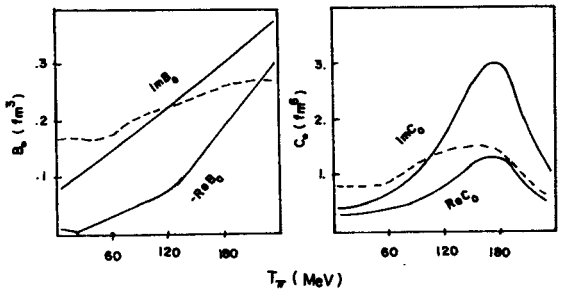

FIG. 1. The s-wave and p-wave absorption parameters. The dashed curve shows the calculated values from Ref. 2.

Sample calculations are shown in Figures 2 and 3. The agreement is typical of what we obtain in this energy region. Note in Fig. 2 that the new absorption parameters improve the fit somewhat. Notice from Fig. 3 that increasing λ does not help much now that we are at higher energy. The theoretical value for λ is less clear at this energy, as the effect of short range nuclear correlations is diminished, so it is possible that the value $\lambda=1$ is reasonable.

Notice that the change in the optical potential also affects the inelastic scattering results. This ambiguity makes it difficult to extract values for β_L from data. Estimates obtained for deformation parameters, as in Ref. 4, can only be compared with other probes after the optical potential is more completely understood at these energies.

The inelastic calculations shown here use standard values for β_L obtained from proton scattering data.

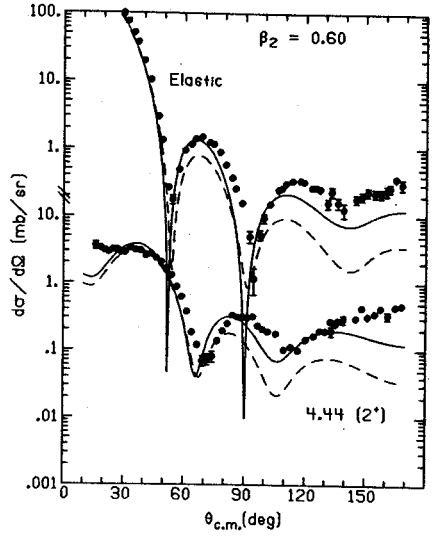

FIG. 2. Calculation for scattering of 163 MeVπ^+ from ^{12}C. The dashed line is calculated using the extrapolated set, while the solid line is calculated with the new absorption parameters from Ref. 2.

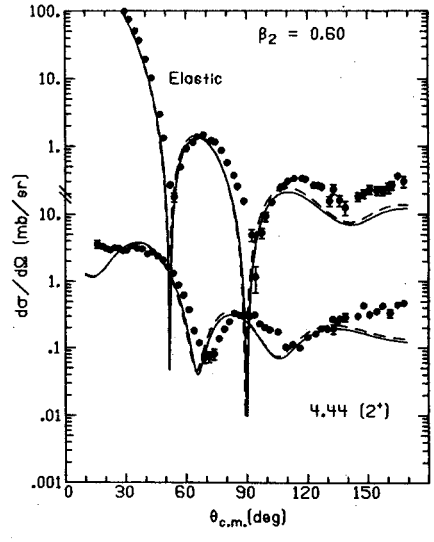

FIG. 3. Calculation from same case as in Fig. 2, where the solid line is calculated with the new set from Ref. 2, while the dashed curve shows the effect of increasing λ from 1.0 to 1.6.

1. K. Stricker, H. McManus and J.A. Carr, Phys. Rev. C19, 929.
2. J. Chai and D.O. Riska, to be published in Nucl. Phys.
3. H. McManus, Second International Conference on Meson-Nuclear Physics, Houston 1979.
4. C. Weidner, et al., Phys. Lett. 78B, 26 (1978).

Second-Order Corrections in Low Energy Pion Nucleus Scattering

J.A. Carr, K. Stricker, and H. McManus

It is well known that terms of second order in the multiple scattering series make important contributions to the pion-nucleus optical potential. In particular, two-body absorption is the dominant process at low energy and is an important part of the optical potential. The Lorentz-Lorenz Ericson-Ericson (LLEE) effect is also important, as it affects the s-p interference minimum that characterizes pion elastic scattering. We are studying how theoretical values for these parameters affect low energy scattering.

In Ref. 1 we used parameters derived from pionic atoms to predict low energy scattering. These pionic atom parameters are listed as Set 1 in Table 1. Recently, calculations of the absorption parameters (Ref. 2) allowed us to reexamine low energy scattering with more theoretical parameters. Discussion of the origin of these new values, listed as Set 2, follows.

We chose to use the phase shift values for the isovector parameters, b_1 and c_1, rather than the fitted pionic values. This change does not affect the resulting cross sections very much.

The absorption parameters, B_0 and C_0, are taken from Chai and Riska (Ref. 2). Unlike Ref. 1, we include $C_0\rho^2$ in the LLEE effect, so we use:

$$\frac{c_0\rho(r) + C_0\rho^2(r)}{1 + \frac{4\pi}{3}\lambda[c_0\rho(r) + C_0\rho^2(r)]}$$

for the p-wave term in the optical potential. This is necessary since short range nuclear correlations are not included in calculating B_0 and C_0.

Since low energy elastic scattering is very sensitive to the interference between s- and p-waves, the new values for ReB_0 and ReC_0 require a change in b_0 and either c_0 or λ to maintain a reasonable fit. The smaller value of ReB_0 requires the larger value of $\bar{b}_0$ in Set 2. The change in sign of ReC_0 requires either a smaller value of c_0 or a larger value of λ. We choose to keep c_0 at its phase shift value of about 0.74. This requires $\lambda = 1.6$, which is consistent with other results (Ref. 3) which comment on the balance between ReC_0 and λ, and place λ in the range 1.2 to 1.6.

Table 1. Optical potential parameters for 50 MeV pion scattering. Set 1 comes from Ref. 1 where C_0 is not included in the LLEE effect, while for set 2 the term in $C_0\rho^2$ is taken inside the LLEE effect. The imaginary parts of b_0, b_1, c_0, c_1 are taken from phase shifts and reduced by a factor to account for the Pauli principle.

	Set 1	Set 2
b_0	-0.04	-0.06
b_1	-0.11	-0.13
c_0	+0.75	+0.74
c_1	+0.62	+0.46
B_0	-0.17 + 0.17i	-0.02 + 0.14i
C_0	-0.79 + 0.79i	+0.36 + 0.59i
λ	1.0	1.6

Several calculations at 50 MeV are shown in Fig. 1. The calculation with the pionic parameters of Set 1 shows qualitative agreement with the data, but the new set shows dramatic improvement, particularly at backward angles.

1. K. Stricker, H. McManus, and J.A. Carr, Phys. Rev. C19, 929 (1979).

2. J. Chai and D.O. Riska, to be published in Nucl. Phys.

3. E. Oset and W. Weise, Nucl. Phys. A319, 477 (1979) and M. Theis, Phys. Lett. 63B, 43 (1976).

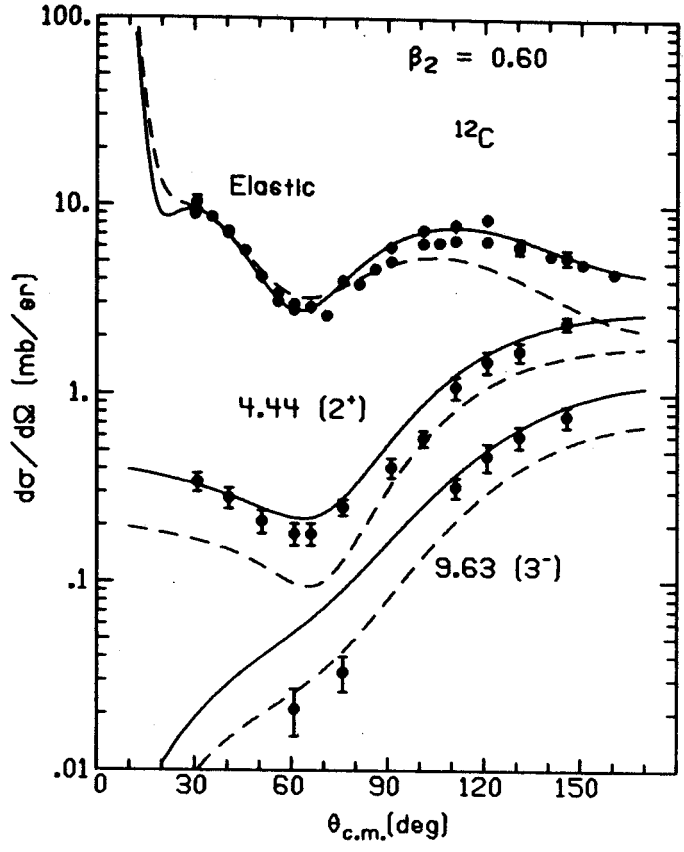
β2 = 0.60
12C
Elastic
4.44 (2+)
9.63 (3-)
dσ/dΩ (mb/sr)
θc.m.(deg)

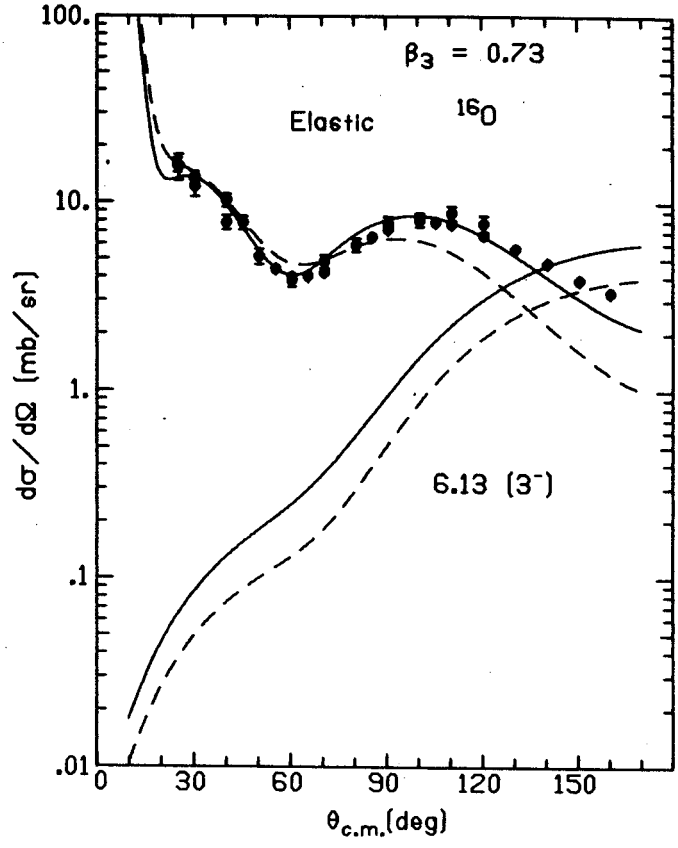
β3 = 0.73
Elastic
16O
6.13 (3-)
dσ/dΩ (mb/sr)
θc.m.(deg)

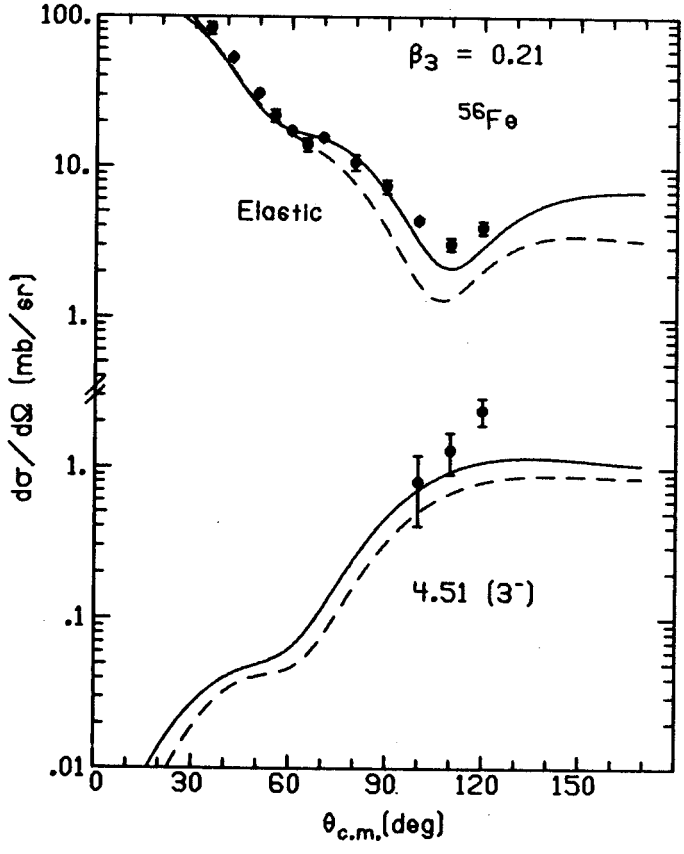
β3 = 0.21
56Fe
Elastic
4.51 (3-)
dσ/dΩ (mb/sr)
θc.m.(deg)

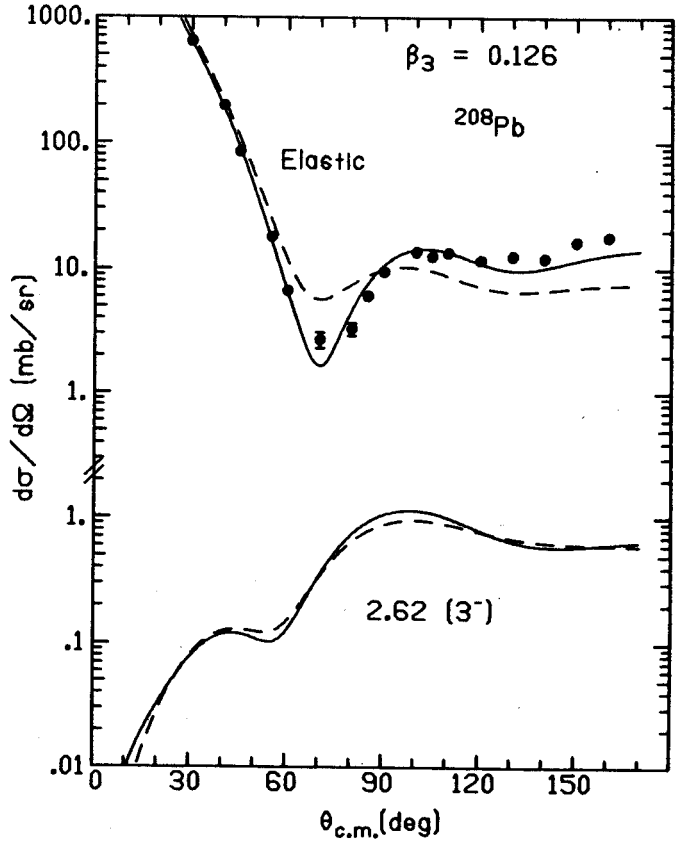
β3 = 0.126
208Pb
Elastic
2.62 (3-)
dσ/dΩ (mb/sr)
θc.m.(deg)

Self Consistency Check of Quasi-Elastic Component of the Pion Potential

J.A. Carr, H. McManus, G.F. Bertsch and G. Richter

The partial cross sections

$$\sigma_{reaction} = \sigma_{quasi\text{-}elastic} + \sigma_{absorption}$$

are more sensitive to particular physical processes of pion scattering than elastic or inelastic scattering. These partial cross sections measure directly the contribution of the various parts of the pion optical potential. We are studying two independent ways of calculating the quasi-elastic cross section as a means of testing the optical potential.

The optical potential derived in Ref. 1 uses the imaginary part of $\bar{b}_0$ and c_0 to account for flux removed from the elastic channel by quasi-elastic scattering. These imaginary parts were taken from phase shifts and then reduced by a factor to account for the effect of the Pauli principle. For low energies the quasi-elastic cross section is approximated by

$$\sigma_{qe} = \frac{-2\omega}{k} \int \phi_a^* \, (\mathrm{Im}\, U_{qe}^{opt}) \, \phi_a \, d^3\underset{\sim}{r} \qquad (1)$$

Where ϕ_a are the distorted waves in the entire optical potential. This cross section is plotted as a solid line in Fig. 1., where the rapid rise with energy can be seen.

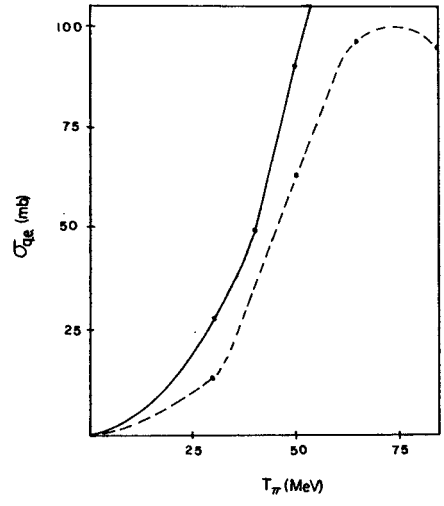

FIG. 1. Graph of quasi-elastic cross section vs. beam energy for π^+ and π^-. The solid curve is calculated from the approximate formula in Equation #1, while the dashed curve is calculated using the response function and the DWIA.

To check this result, we calculated the quasi-elastic cross section directly using the DWIA and the nuclear response function for ^{40}Ca. The response function is computed (Ref. 2) by first determining the single-particle states in ^{40}Ca using a Hartree-Fock calculation. These states are then used to generate an RPA Greens function. The Green's function is then converted to the form $d\beta_L^2/dE$ for use in the distorted wave calculations.

The resulting $d\sigma/dE$ is shown in Fig. 2 for 30, 50, 65 MeV π^+ ^{40}Ca. The low energy peak is composed of the collective 3^- and 5^- states, while the bump in the 16-20 MeV region is due to the giant quadrupole and 4^+ collective states. Isovector states contribute about 15% of the cross section. It is interesting to observe how the rise in the quasi-elastic cross section is produced, in part, by the increased contribution of high excitation states as the beam energy increases.

These results for σ_{qe} are plotted as the dashed curve in Fig. 1. Notice that the trends are reproduced although the magnitudes are different. The magnitude is less important since the response function was not fitted to electron scattering. This independent result tends to confirm the values of the Pauli factor used to obtain the quasi-elastic component of the pion optical potential.

---

1. K. Stricker, H. McManus, J.A. Carr, Phys. Rev. C19, 929 (1979).
2. G.F. Bertsch and S.F. Tsai, Phys. Rev. 18C, 126 (1975).

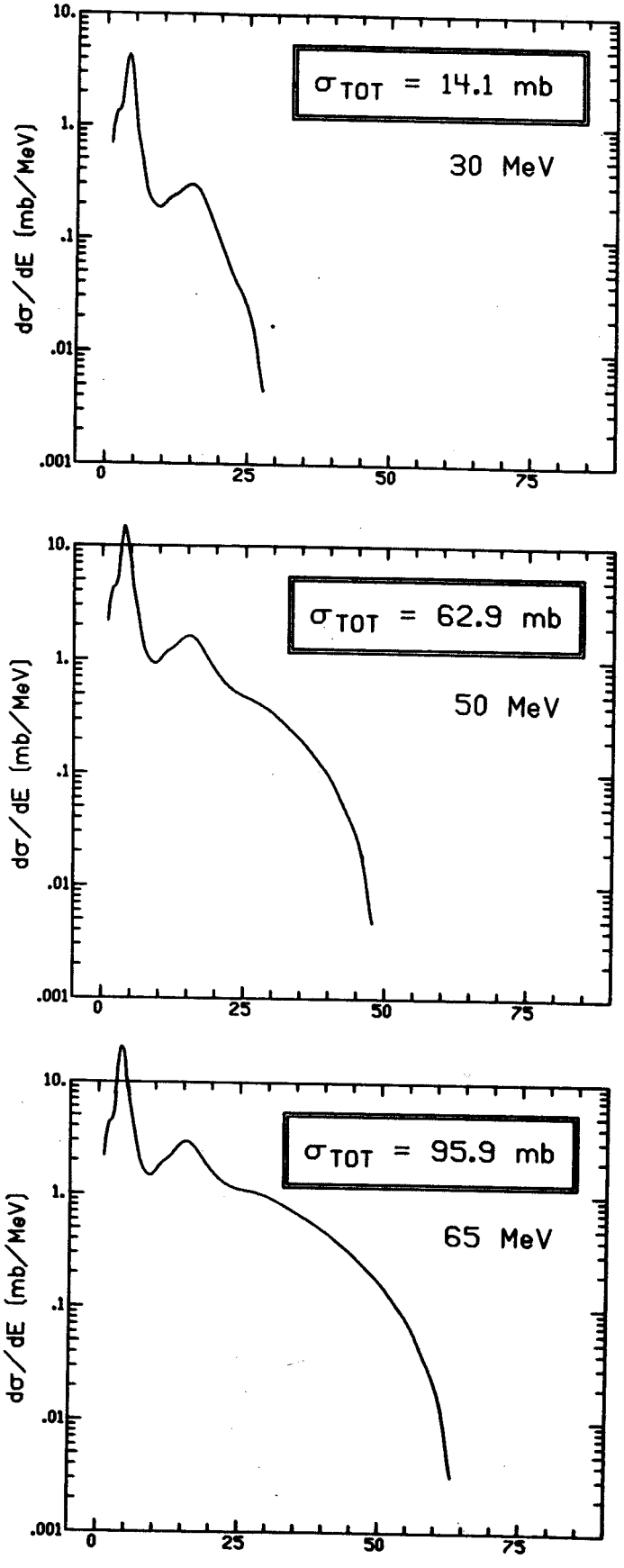
σTOT = 14.1 mb
30 MeV
σTOT = 62.9 mb
50 MeV
σTOT = 95.9 mb
65 MeV
dσ/dE (mb/MeV)
10.
1.
.1
.01
.001
0
25
50
75
Excitation Energy (MeV)

Transverse Form Factors

Dongwoo Cha

The theory of the transverse electromagnetic form factor of nuclei has not been adequately studied. In the shell model representation, the matrix elements of momentum operators are more difficult to calculate reliably than the matrix elements of the density operators. For example, for the ^{12}C $0^+ \rightarrow 2^+$ (4.44) transition, the convection current vanishes with usual wavefunctions. This is a defect of the wavefunctions; the equation of continuity requires a substantial convection current at momentum transfer $q \lesssim 1$ fm^{-1}. We have explicitly added a convection current to the spin contribution to the ^{12}C transition, to account for the experimental data.[1] This is shown in Fig. 1. We are now developing a theory of the transverse form factor which is automatically consistent with the equation of continuity. To achieve this, we augment the usual shell model wavefunctions by perturbation theory. We will also require electromagnetic transition operators to have a two-body character. This is needed for consistency with the non-local residual interaction.

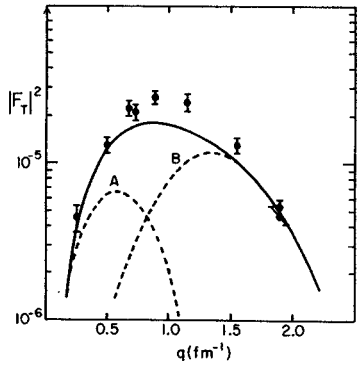

Fig. 1. Transverse form factor for ^{12}C $0^+ \rightarrow 2^+$ (4.44). Data is shown as dots. Curve A is the contribution of the convection current; curve B is an assumed spin contribution; the solid line is the coherent sum of the two.

---

1. D. Cha, submitted to Phys. Rev.